The Unusual Intersubunit Ferroxidase Center of *Listeria innocua* Dps Is Required for Hydrogen Peroxide Detoxification but Not for Iron Uptake. A Study with Site-Specific Mutants[†,‡]

Andrea Ilari,[§] Maria Carmela Latella,[§] Pierpaolo Ceci,[§] Federica Ribacchi,[§] Meihong Su,[||] Laura Giangiacomo,[§] Simonetta Stefanini,[§] N. Dennis Chasteen,[||] and Emilia Chiancone*[,§]

Istituto di Biologia e Patologia Molecolari CNR, Dipartimento di Scienze Biochimiche, Università La Sapienza, P.le A. Moro, 5, 00185 Roma, Italy, and Department of Chemistry, University of New Hampshire, Durham, New Hampshire 03824

Received January 3, 2005; Revised Manuscript Received February 17, 2005

ABSTRACT: The role of the ferroxidase center in iron uptake and hydrogen peroxide detoxification was investigated in *Listeria innocua* Dps by substituting the iron ligands His31, His43, and Asp58 with glycine or alanine residues either individually or in combination. The X-ray crystal structures of the variants reveal only small alterations in the ferroxidase center region compared to the native protein. Quenching of the protein fluorescence was exploited to assess stoichiometry and affinity of metal binding. Substitution of either His31 or His43 decreases Fe(II) affinity significantly with respect to wt *L. innocua* Dps ($K \sim 10^5$ vs $\sim 10^7$ M^{-1}) but does not alter the binding stoichiometry [12 Fe(II)/dodecamer]. In the H31G-H43G and H31G-H43G-D58A variants, binding of Fe(II) does not take place with measurable affinity. Oxidation of protein-bound Fe(II) increases the binding stoichiometry to 24 Fe(III)/dodecamer. However, the extent of fluorescence quenching upon Fe(III) binding decreases, and the end point near 24 Fe(III)/dodecamer becomes less distinct with increase in the number of mutated residues. In the presence of dioxygen, the mutations have little or no effect on the kinetics of iron uptake and in the formation of micelles inside the protein shell. In contrast, in the presence of hydrogen peroxide, with increase in the number of substitutions the rate of iron oxidation and the capacity to inhibit Fenton chemistry, thereby protecting DNA from oxidative damage, appear increasingly compromised, a further indication of the role of ferroxidation in conferring peroxide tolerance to the bacterium.

When first characterized, *Listeria innocua* Dps[1] (*D*NA-binding *p*roteins from *s*tarved cells) was named ferritin since it does not bind DNA but resembles closely mammalian ferritins in terms of iron oxidation/uptake capacity (*1*). Later studies showed that other members of the Dps family are unable to bind DNA [e.g. Dlp-1 and Dlp-2 from *Bacillus anthracis* (*2*), HP-NAP from *Helicobacter pylori* (*3*) and *Agrobacterium tumefaciens* Dps (*4*)], whereas all Dps proteins are endowed with some ferritin-like properties. Most importantly, these proteins play a major role in the protection of DNA from oxidative damage and in conferring resistance to hydrogen peroxide stress in vivo (*5*−*9*).

In Dps proteins the iron oxidation/uptake process has distinctive features relative to canonical ferritins. The most relevant one was revealed by the *L. innocua* Dps X-ray crystal structure (*10*). It concerns the ferroxidase center, the site where Fe(II) is oxidized catalytically in the first step of the process of iron deposition in the protein. Whereas all known ferroxidase centers are dinuclear sites embedded within the four-helix bundle of an individual polypeptide chain, in Dps proteins the ferroxidase center has an unusual location at the interface of 2-fold symmetry-related subunits such that the iron ligands are contributed by both symmetry-related monomers (*10*, *11*). In canonical ferritins, the bound iron atoms are at a distance of about 3 Å and are connected by an oxo-bridge. The so-called A site typically uses a histidine residue and carboxylates as iron coordinating ligands and binds iron with higher affinity than the so-called B site where the metal is coordinated only by means of carboxylates. In the X-ray crystal structure of *Listeria* Dps, the ferroxidase center contains one bound iron coordinated by Glu62 and Asp58 from one subunit, by His31 from the symmetry-related one, and by a water molecule, at about 3 Å from the iron, that forms a hydrogen bond with His43 from the same monomer. A diiron site was modeled, in which the second iron atom replaces the water molecule and hence is coordinated by His43, while Glu62 provides the oxo-bridge between the two metal ions (*10*). Importantly, the iron ligands are highly conserved throughout the Dps family. In accord with the dinuclear nature of the unusual intersubunit ferroxidase center, iron deposition in *Listeria* Dps is initiated by the oxidation of two Fe(II) per monomer. In contrast with

[†] This work was supported by Grant MIUR PRIN 2002 (S.S.), Fondazione Pasteur Cenci-Bolognetti and Grant MIUR PRIN 2003 (E.C.), and NIH Grant R01 GM 20194 (N.D.C.).

[‡] The atomic coordinates of the *Listeria innocua* Dps mutants have been deposited with the Protein Data Bank (accession code: 2BK6 for H31G; 2BKC for H43G; 2BJY for H31G-H43G).

* To whom correspondence should be addressed. Phone: +39-06-49910761. Fax: +39-06-4440062. E-mail: emilia.chiancone@uniroma1.it.

[§] Università La Sapienza.

[||] University of New Hampshire.

[1] Abbreviations: Dps, *D*NA-binding *p*rotein from *s*tarved cells; EcFtnA, *E. coli* bacterial ferritin type A; ITC, isothermal titration calorimetry; Mops, 3-(*N*-morpholino)propanesulfonic acid.

10.1021/bi050005e CCC: $30.25
Published on Web 03/23/2005

Table 1: Oligonucleotides for the PCR Reactions

primer	sequence
A1	5′-GGA GGA AGA T**AC ATA TG**A AAA CAA TC-3′
B2	5′-GTT TT**G GAT CC**A TCT TAT TCT AAT GG-3′
H43f2	5′-GGC CAC AAC TTC TTC ACT TTA **GGT** GAA AAA ATG GAT GAT TTA TAT AGC G-3′
H43r	5′-CGC TAT ATA AAT CAT CCA TTT TTT C**AC C**TA AAG TGA AGA AGT TGT GGC C-3′
H31f	5′-CGT ATT CAC AGT AAA AAT TCA TCA AAT T**GG T**TG GTA TAT GCG AGG CC-3′
H31f2	5′-CAA ATT GGT TGG TAT ATG CG-3′
H31r	5′-GGC CTC GCA TAT ACC A**AC C**AA TTT GAT GAA TTT TTA CTG TGA ATA CG-3′
H31r2	5′-CGC ATA TAC CAA CCA ATT TG-3′
D58f	5′-GTG AAC AAA TGG **CTG** AAG TAG CAG AAC TG-3′
D58r	5′-CAG TTC TGC TAC TTC **AGC** CAT TTG TTC AC-3′
T7pro	5′-TAA TAC GAC TCA CTA TAG G-3′
T7term	5′-GCT AGT TAT TGC TCA GCG-3′

canonical ferritins, the oxidation of the ferroxidase site complex by dioxygen in *Listeria* Dps proceeds more slowly than the oxidation/mineralization phase that takes place inside the protein shell (*12*). In fact, hydrogen peroxide is a better Fe(II) oxidant than dioxygen, a property related to the peroxide tolerance conferred by Dps proteins (*5*−*9*).

The present study of site-specific mutants of the *Listeria* Dps ferroxidase center was undertaken to obtain insight into the possible reasons for these differences and to better define the relationships between its structural and functional properties. In human H-chain ferritin and *Escherichia coli* ferritin (EcFtnA), the behavior of site-specific mutants with altered A and B site ligands indicated that modification of site A interferes with Fe(II) binding, whereas modification of site B drastically inhibits oxidation without preventing Fe(II) binding at site A. Site A was thought to be preferred for Fe(II) binding due to the presence of mixed oxygen and nitrogen ligands (*13*, *14*). This situation does not apply to *Listeria* Dps where both the A and the proposed B sites contain a histidine ligand, namely, His31 and His43. To establish their contribution to the functionality of the ferroxidase center, these histidine residues were replaced by glycine either individually in the H31G and H43G mutants or together in the double mutant H31G-H43G. An additional A site iron ligand, Asp58, was substituted by alanine in the triple mutant, H31G-H43G-D58A.

The structural and functional characterization of the site-specific mutants shows that modifications of the ferroxidase center do not affect the iron oxidation/uptake properties of *Listeria* Dps significantly when dioxygen is the oxidant. However, with hydrogen peroxide as the oxidant, such modifications significantly reduce the rate of Fe(II) oxidation and diminish the hydrogen peroxide detoxification capacity of the protein and hence provide yet another proof of the relevance of Dps proteins in conferring hydrogen peroxide tolerance.

MATERIALS AND METHODS

Plasmid Construction. Recombinant *L. innocua* ferritin was overexpressed in *E. coli* strain BL21(DE3). The gene, *fri*, was obtained by means of PCR techniques using pTZ35 as template (*15*) and primers A1 (forward primer) and B2 (reverse primer) containing the cleavage sites for restriction enzymes *Nde*I and *Bam*HI (Table 1). The resulting 468-bp product was doubly digested with *Nde*I and *Bam*HI, isolated using the QIAquick gel extraction kit (Qiagen), and subcloned into the expression vector pET-11a (Novagen).

The His31 → Gly mutant (H31G) was generated by the PCR technique with the wild-type *fri* gene as template. H31f and H31r (Table 1) were used as forward and reverse primers, respectively. PCR reactions were performed by the Qiagen method using Pfu Turbo DNA polymerase (Stratagene).

The His43 → Gly mutant (H43G) was generated by three-stage PCR utilizing A1 and H43r as primers for PCR1 and H43f2 and B2 for PCR2 (Table 1). Equimolar amounts of the PCR1 and PCR2 fragments were utilized to carry out the third PCR reaction (PCR3) with oligonucleotides A1 and B2.

The double mutant His31 → Gly,His43 → Gly (H31G-H43G) was constructed with the same method utilized for the H43G mutant which was used as template. Two PCR reactions were performed with primers H31f2 and T7 terminator for PCR1 and the T7 promoter and H31r2 for PCR2 (Table 1). Further amplification (PCR3) was performed using the T7 promoter and T7 terminator.

The triple mutant His31 → Gly,His43 → Gly,Asp58 → Ala (H31G-H43G-D58A) was generated using the double mutant as template. Three different PCR reactions were performed utilizing primers A1 and D58r (PCR1), B2 and D58f (PCR2), and equimolar amounts of the PCR1 and PCR2 products for PCR3 containing the A1 and B2 primers (Table 1).

All PCR fragments are digested with *Nde*I and *Bam*HI and cloned into pET-11a. All products were purified with the Qiagen kit; the purified DNA was transformed into *E. coli* strain BL21(DE3). The variant constructs were confirmed by DNA sequencing.

Protein Purification and Characterization. The recombinant wild-type (wt) protein and the site-specific mutants were purified essentially as described by Bozzi et al. (*1*) with one modification. The gel filtration step was substituted by ion-exchange chromatography on a DEAE-52 column equilibrated with 20 mM Tris-HCl buffer at pH 7.8. The wt protein and its site-specific mutants were eluted with a 0.1−0.3 M NaCl gradient.

The wt protein contains 1.8−2.0 Fe/dodecamer as assessed by atomic absorption spectroscopy or the ferrozine method (Fluka), whereas the variants are iron-free. Protein concentration was determined spectrophotometrically on the basis of the molar (M_r 216 kDa) absorption coefficient, $\epsilon = 2.59 \times 10^5$ M^{-1} cm^{-1} at 280 nm (*1*).

Circular dichroism spectra were recorded on a Jasco J-720 spectropolarimeter. Near-UV CD (250−350 nm) measurements were performed on 4.5 μM protein solutions in 50

Table 2: Crystallographic Data Statistics

parameter	H31G	H43G	H31G-H43G
	Data Scaling		
data resolution (Å)	2.2	2.3	2.6
completeness (%)	97.7	91.5	94%
R_{merge} (%)	9.9	7.5	9.9
space group	$I4_122$	$P2_1$	$P2_12_12_1$
unit cell content	hexamer	2 dodecamers	dodecamer
cell dimensions			
a (Å)	136.33	90.73	86.6
b (Å)	136.33	175.65	132.2
c (Å)	242.49	135.96	168.0
β (deg)	90	92.52	90
	Refinement Statistics		
R_{crys} (%)	21	20.8	21
R_{free} (%)	23	26.5	25
rms deviation			
bonds (Å)	0.016	0.018	0.019
angles (deg)	1.9	1.6	2.1
residues in most favored regions of Ramachandran plot (%)	96.6	96.3	97.1

mM Mops−NaOH, pH 7.0. The results are expressed as molar ellipticity assuming a mean residue weight of 110 per amino acid residue.

Protein Crystallization. Crystallization of the H31G, H43G, and H31G-H43G mutants was achieved at 293 K by the hanging drop vapor diffusion technique. A 2 μL volume of the protein sample (32 μM), equilibrated against 30 mM Tris-HCl, pH 7.5, and 200 mM NaCl, was mixed with an equal amount of the reservoir solution containing 0.1 M acetate buffers at pH values between 5.5 and 6.5 and PEG 1000 in the range of 15−30% (w/v). The H31G, H43G, and H31G-H43G crystals grew in 1 week and showed different morphologies.

Data Collection and Processing. Data were collected as 1.0 oscillation frames using the MAR CCD detector on the X-ray beamline at ELETTRA, Basovizza (Trieste, Italy) at a wavelength of 1.0 Å. Data were collected at 100 K using 10−15% PEG 200 as cryoprotectant. The data analysis, performed with DENZO (*16*), indicates that the crystals belong to different space groups: the H31G-H43G crystals being orthorhombic (space group $P2_12_12_1$; $a = 86.6$ Å, $b = 132.2$ Å, $c = 168.0$ Å), the H31G crystals being tetragonal (space group $I4_122$; $a = 136.33$ Å, $b = 136.33$ Å, $c = 242.48$ Å), and the H43G crystals being monoclinic (space group $P2_1$; $a = 90.72$ Å, $b = 175.648$ Å, $c = 135.957$ Å, $\beta = 92.52$). The data were scaled using SCALEPACK (*16*); data scaling statistics are presented in Table 2.

Structure Solution and Refinement. The structures were solved by molecular replacement using as search probe native *L. innocua* ferritin (RCSB entry 1qgh). The rotational and translational searches, performed with the program AmoRe (*17*) in the resolution range of 10−3.0 Å, produced clear solutions. Refinement of the atomic coordinates and displacement parameters was carried out by the maximum likelihood method with the program REFMAC (*18*). The refinement statistics are presented in Table 2. Model building was performed using the program package XTALVIEW (*19*). Water molecules were added to the model manually. The quality of the model was assessed by the program PROCHECK (*20*).

Fe(II) and Fe(III) Binding. Fluorescence measurements were carried out on a Fluoromax (Spex Industry) or a Varian Cary Eclipse fluorometer. Anaerobic titrations with Fe(II) and Fe(III) were carried out in gastight cells (path length = 1 cm) under a nitrogen or argon atmosphere. Freshly prepared anaerobic 3 mM ferrous ammonium sulfate solutions were added in increments of 12 Fe(II) up to 72 Fe(II)/dodecamer. Anaerobic titrations with Fe(III) were performed in a gastight quartz cell under an argon atmosphere with the incremental addition of 4 Fe(II)/dodecamer followed by 0.5 H_2O_2/Fe(II) each time.

The Fe(II) oxidation and Fe(III) hydrolysis reactions were followed using a specially designed 600 μL cell fitted with Clark-type oxygen and a combination glass−Ag/AgCl pH microelectrode. The apparatus enables one to measure simultaneously the kinetics of both oxygen consumption and proton production under buffer-free conditions as well as the stoichiometry of the reaction when Fe(II) is introduced into the protein to initiate iron oxidation and mineralization. The procedures and standardization reactions of the oxygen electrode/pH stat apparatus are described in detail elsewhere (*21*).

Iron Incorporation. Iron incorporation experiments were performed by addition of freshly prepared anaerobic ferrous ammonium sulfate solutions (10 mM) to air-equilibrated protein solutions (5.5 μM) in 50 mM Mops−NaOH, pH 7.0. Fe(II) was added in increments corresponding to 12 or 24 Fe/dodecamer. The kinetics of iron oxidation and uptake were followed at 25 °C by measuring the absorbance of the ferric hydrous oxide micelle at either 304 or 310 nm using the molar absorption coefficient, $\epsilon = 450$ (*22*). The solutions were maintained under continuous stirring during the course of the experiments. As a control, the rate of Fe(II) autoxidation was measured in parallel.

Sedimentation velocity experiments were carried out to assess the distribution of micellar iron after addition of 150 Fe/dodecamer to 1 μM solutions of the wt protein and its variants in 50 mM Mops−NaOH, pH 7.0. The experiments were conducted at 30000 rev/min and 20 °C in a Beckman Optima XL-A analytical ultracentrifuge equipped with absorbance optics. Data were collected at 280 and 310 nm and analyzed with the program Sedfit. The sedimentation coefficients were reduced to $s_{20,w}$ by standard procedures.

DNA Protection Assay. DNA protection from oxidative damage was assessed in vitro using pET-11a plasmid DNA (5600 bp, 20 nM), purified by a Qiaprep spin plasmid miniprep kit (Qiagen). The total volume reaction was 12 μL in 30 mM Tris-HCl and 150 mM NaCl, pH 7.3. The wt protein and its site-specific mutants (3 μM) were allowed to interact with DNA for 10 min prior to introduction of variable amounts of $FeSO_4$ and H_2O_2 in large molar excess over iron. The reaction mixtures were incubated for 3 min at room temperature to allow oxidation and mineralization of added iron (*23*) and thereafter were treated with 2% SDS at 85 °C for 5 min. Plasmid DNA was resolved by electrophoresis on 1% agarose gel. The gel was stained with ethidium bromide, imaged by ImageMaster VDS, and quantitated using the Image Master Total Lab software.

Protection against Fe(II)-Mediated Hydroxyl Radical Formation. The fluorometric assay described by Yamamoto et al. (*24*) and Ceci et al. (*4*) was used. It is based on the Fe(II)-mediated production of hydroxyl radicals that degrade

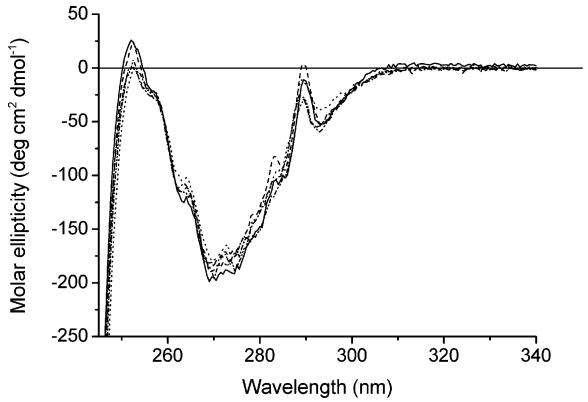

FIGURE 1: Near-UV circular dichroism spectra of *L. innocua* Dps and its ferroxidase center variants. The protein concentration was 4.5 μM in 50 mM Mops−NaOH buffer, pH 7.0. Key: wt Dps (—); H31G (- - -); H43G (• • •); H31G-H43G (— • —); H31G-H43G-D58A (— •• —). All the spectra were recorded at 20 °C.

deoxyribose to a fluorescent chromogen. The chromogen fluorescence at 553 nm (λ_{ex} 532 nm) was measured in 30 mM potassium phosphate buffer at pH 7.4 containing 63 mM NaCl, 1 mM deoxyribose, and 22 μM ferrous ammonium sulfate. *Listeria* Dps and its ferroxidase center variants were at a concentration of 0.22 μM.

RESULTS

Structural Characterization in Solution and in the Crystal. The solution properties of the *Listeria* Dps variants under study are essentially the same as those of the native and recombinant wt protein. Thus, all proteins sediment as dodecamers in the ultracentrifuge ($s_{20,w} \sim 10.5$ S), and their absorption and far-UV CD spectra are superimposable (data not shown). The near-UV CD spectra likewise are very similar, apart from a small difference in the peak at about 253 nm whose ellipticity has a positive value only in the wt and H31G proteins (Figure 1). The fluorescence emission of all variants displays a small red shift (λ_{max} 338−340 nm) relative to the wt protein (λ_{max} 334 nm).

In accord with the spectroscopic data in solution, the X-ray crystal structures of the native and variant proteins are all very similar as indicated by the superpositions of the respective Cα positions which yield root-mean-square deviations (rms) between 0.964 and 1.091 Å. Distinct differences are apparent only in the ferroxidase center regions. In the native protein (Figure 2A), site A contains one iron ion ligated by Asp58 (OD1) and Glu62 (OE2) located on one subunit, by His31 (NE2) located on the symmetry-related monomer, and by a water molecule (w35), indicated as Wb in the figure and in Table 3, that lies about 3 Å from the iron and is hydrogen bonded to His43 from the latter monomer. In the dinuclear site the second iron is believed to replace this water molecule. Notable features of the center are (i) the salt bridge ($d = 2.9$ Å) formed by OE1 of Glu62 with Nz of Lys141 which belongs to a subunit related by 3-fold symmetry to the subunit containing His31 and His43, (ii) the hydrogen bond between the iron ligand Asp58 (OD2) and Trp32 (NE1), (iii) the presence of an additional aspartate (Asp47) at 3.7 Å from the iron that may contribute to compensate its positive charge, (iv) the location of His43 near Asp47 and Glu44, two carboxylates facing the internal

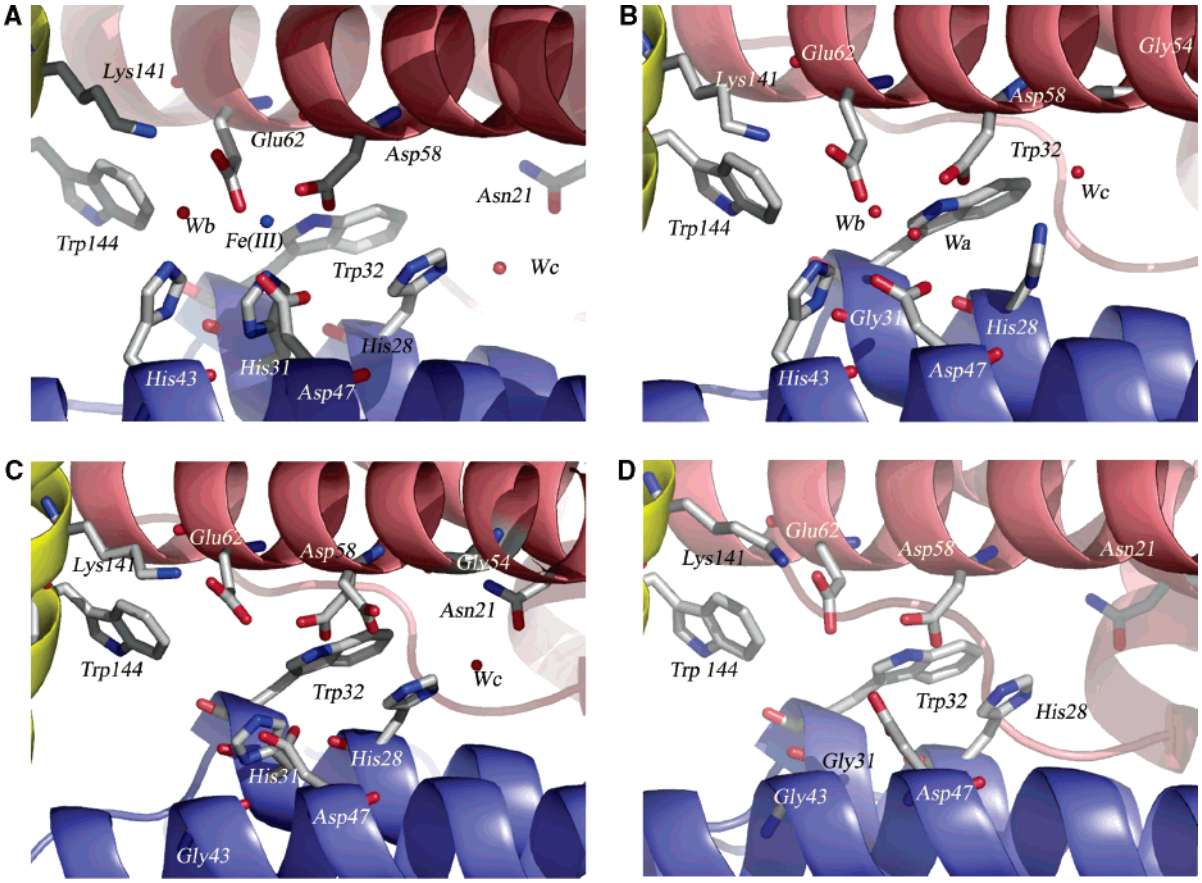

FIGURE 2: X-ray crystal structure of the ferroxidase center in *L. innocua* Dps and its ferroxidase center variants. Panels: (A) native Dps; (B) H31G; (C) H43G; (D) H31G-H43G. The pictures were generated by the program PyMol (*28*).

Table 3: Relevant Distances (in Å) in the Ferroxidase Center of wt *Listeria* Dps and Its Variants H31G, H43G, and H31G-H43G[a]

	WT	H31G	H43G	H31G-H43G
$Glu^{62}OE1-Lys^{41}NZ$	3.0	3.8	3.4	3.4
$Glu^{62}OE2-Wa$	2.2	2.5		
$Asp^{58}OD1\text{-}A-Trp^{32}NE1$	2.8	3.0	2.7	2.6
$Asp^{58}OD1\text{-}A-Fe(III)/Wa$	1.8	2.8		
$Asp^{58}OD1\text{-}A-Glu^{62}OE2$			2.22	2.69
$Asp^{58}OD2\text{-}A-Wa$		3.0		
$Asp^{58}OD2\text{-}A-Wb$		3.2		
$Asp^{58}OD1\text{-}B-His^{28}NE$			2.7	
$Asp^{58}OD2\text{-}B-Gly^{54}O$			2.7	
$Asp^{58}OD2\text{-}B-Glu^{62}OE2$			2.22	
$His^{31}NE2-Fe(III)/Wa$	2.4			
$His^{43}NE2-Wb$	2.5	3.9		
$His^{28}NE2-Wc$		3.0		3.7
$Asp^{47}OD1-Wc$	3.8	2.9		3.7
$Asp^{47}OD1-Wa$		2.8		
$Asp^{47}OD2-Wb$		2.7		
$Wa/Fe(III)-Wb$	3.0	3.3		
$Wc-Wa$		3.9		

[a] A indicates the conformation adopted by the Asp^{58} side chain in the native protein; B indicates the alternative conformation adopted in the H43G mutant.

cavity of the protein shell that could provide the nucleation sites for iron micelle formation, and (v) the presence of a third water molecule (Wc in the figure and in Table 3) hydrogen bonded to His28 and Asn21 in a position that may be occupied by Fe(II) in transit to the ferroxidase site.

The replacement of His31 with glycine (Figure 2B) leads to a reorganization of the ferroxidase center without large alterations in the interaction network just described. In H31G, Asp47 lies nearer to the site A iron ligands, Asp58 and Glu62, as compared to the native protein. The ferroxidase center contains three water molecules (see Table 3): Wb, in the B site near His43 as in the native protein, Wa replacing the iron atom in the A site, and Wc placed near site A (d = 6.7 Å) in a position similar to that occupied in the native protein. A hydrogen bond network links the water molecules as follows: Wa is bonded to OD2 of Asp58 (d = 3.0 Å), to OE2 of Glu62 (d = 2.6 Å), to OD1 of Asp47 (d = 2.84 Å), and to Wb (d = 3.27 Å); Wc is bonded only to His28 (Table 3). In turn, compared to the native protein where iron is in the place of Wa, all of the distances between Wa and the iron ligands are increased as well as the distance between Wb and His43 (d = 3.9 Å). Further, Trp32 lies at 3.1 Å from Asp58 as compared to 2.5 Å in the native protein.

The ferroxidase center in H43G (Figure 2C) and in the double variant H31G-H43G (Figure 2D) contains no iron or water molecules. However, in H43G, there is a water molecule (Wc) near the ferroxidase center, in the same position as in the native protein. Most interestingly, in the H43G protein, Asp58 can clearly adopt two configurations: in one (configuration A) it is hydrogen bonded to Trp32 and to Glu62 such that the site architecture resembles that of the native protein despite the absence of the metal; in the other (configuration B) Asp58 forms a hydrogen bond with His28. In the double variant H31G-H43G, the two iron ligands, Asp58 and Glu62, are positioned as in the native protein such that the distances between Asp58 and Trp32 and between Glu62 and Lys 141 are practically unaltered.

Fe(II) Binding Stoichiometry and Proton Release. The quenching of the intrinsic protein fluorescence was used to follow Fe(II) binding to the ferroxidase center given its short distance from the tryptophan residues (<5 Å). The Fe(II) complex does not absorb in the spectral region of tryptophan emission so quenching is largely attributed to paramagnetism of the Fe(II) itself. It should be recalled that the wt protein contains 1.8−2.0 Fe/dodecamer whereas the variants are iron-free.

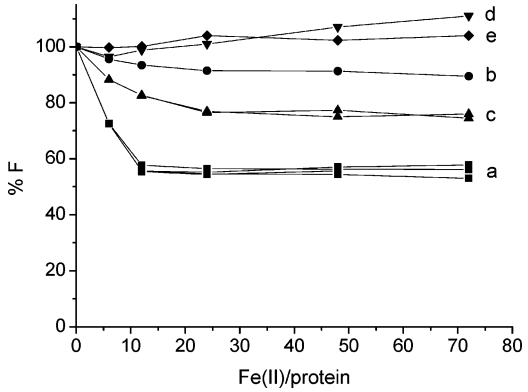

FIGURE 3: Fluorimetric titration in anaerobiosis of *L. innocua* Dps and its ferroxidase center variants with Fe(II). Curves: (a) wt Dps; (b) H31G; (c) H43G; (d) H31G-H43G; (e) H31G-H43G-D58A. The protein concentration was 1.5 μM in 50 mM Mops−NaOH buffer, pH 7.0. All of the spectra were recorded at 300−400 nm and 25 °C. Excitation was at 290 nm.

In wt Dps quenching reaches a maximum upon anaerobic addition of 12 Fe(II)/polymer, whereas in the H43G and H31G variants, fluorescence decreases monotonically, albeit to a different extent, with increase in Fe(II) concentration (Figure 3). The apparent affinity constant K for Fe(II) binding to the wt protein has been determined by isothermal titration calorimetry (ITC) to be $\sim 10^7$ M^{-1} (*23*). In the case of the single mutants, we estimate K to be $\sim 10^5$ M^{-1} from the Fe(II) concentration producing half-maximal fluorescence quenching in Figure 3. In wt Dps Fe(II) binding is accompanied by a blue shift of the emission maximum (λ_{max} 334−330 nm). In both single mutants λ_{max} is at 338 nm and shifts to 336 nm only in the H43G protein. In the double and triple mutants, H31G-H43G and H31G-H43G-D58A, the intrinsic fluorescence, characterized by λ_{max} at 340 nm, is essentially unaffected by Fe(II).

In a different type of experiment the proton production associated with Fe(II) binding to the ferroxidase center was assessed. To this end, the number of protons liberated at pH 7.0 upon anaerobic titration with Fe(II) of *L. innocua* Dps and its variants was measured by autotitration with standard NaOH (5.0 mM) using the pH stat apparatus. Electrode oximetry was used simultaneously to ensure that the solution remained anaerobic throughout the experiment (*21*). The resultant H^+/Fe(II) stoichiometries for Fe(II) loadings in two steps of 12 Fe/dodecamer are listed in Table 4. With the wt protein, $\sim$1 H^+ is liberated per Fe(II) added for the first 12 Fe(II)/dodecamer whereas minimal H^+ production is observed for the second addition of 12 Fe(II)/dodecamer, a result in accord with the binding of 12 Fe(II) to the protein as established by ITC and fluorescence titrations (*23*). The coordinating His31 and/or His43 residues of the ferroxidase center are most likely the source of the protons. For the single mutants H31G and H43G, $\sim$1 H^+ is released per Fe(II) added for the first 12 Fe(II)/dodecamer, dropping to $\sim$0.2 H^+/Fe(II) for the second 12 Fe(II)/dodecamer addition, an observa-

Table 4: Specific $H^+/Fe(II)$ Stoichiometries upon Fe(II) Binding to *Listeria* Dps and Its Variants H31G, H43G, H31G-H43G, and H31G-H43G-D58A under Different Fe(II)/Dodecamer Loadings[a]

protein	H^+/Fe^{2+} stoichiometry	
	first 12 Fe^{2+}/ dodecamer	second 12 Fe^{2+}/ dodecamer
wt	1.04 ± 0.16 ($N = 7$)	0.16 ± 0.01 ($N = 2$)
H31G	1.11 ± 0.06 ($N = 4$)	0.13 ± 0.03 ($N = 3$)
H43G	0.92 ± 0.05 ($N = 5$)	0.21 ± 0.08 ($N = 4$)
H31G-H43G	0.22 ± 0.11 ($N = 4$)	0.20 ± 0.05 ($N = 3$)
H31G-H43G-D58A	0.18 ($N = 1$)	0.17 ± 0.03 ($N = 2$)

[a] Conditions: 2.0 μM protein in 3 mM Mops and 100 mM NaCl, pH 7.3, pH stat proportional band = 0.5, and tritation speed = 80 or 60; N is the number of determinations.

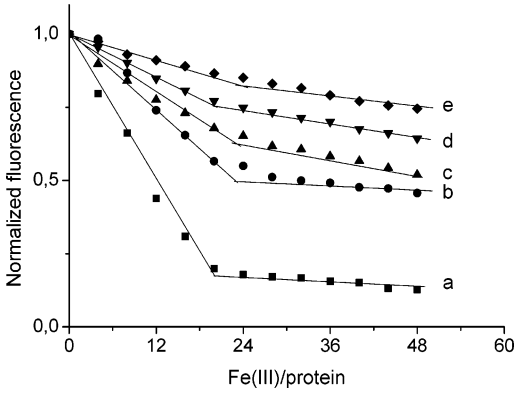

FIGURE 4: Fluorescence titration of *L. innocua* Dps and its ferroxidase center variants with Fe(III). Curves: (a, ■) wt Dps, 1.1 μM; (b, ●) H31G, 1.2 μM; (c, ▲) H43G, 1.5 μM; (d, ▼) H31G-H43G, 1.5 μM; (e, ◆) H31G-H43G-D58A, 1.4 μM. Each point corresponds to the addition of 4 Fe(II)/protein followed by 0.5 H_2O_2/Fe(II). Conditions were as follows: $\lambda_{ex} = 280$ nm, $\lambda_{em} = 335$ nm, slits for both excitation and emission were 5 nm, anaerobic, 100 mM Mops, 0.05 M NaCl, pH 7.0.

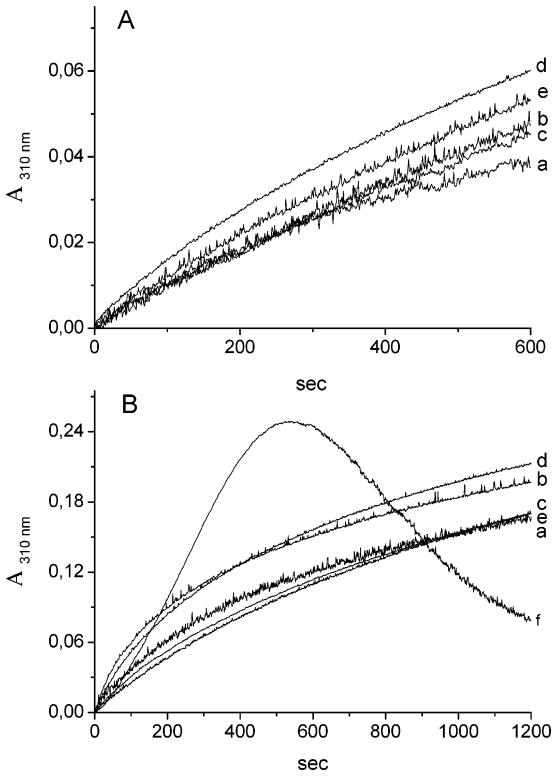

FIGURE 5: Progress curves of iron uptake by *L. innocua* Dps and its ferroxidase center variants after addition of 12 (A) and 24 (B) Fe(II) per dodecamer in the presence of dioxygen. Curves: (a) wt Dps; (b) H31G; (c) H43G; (d) H31G-H43G; (e) H31G-H43G-D58A; (f) iron autoxidation. The protein concentration was 6.0 μM in 50 mM Mops−NaOH buffer, pH 7.0. The temperature was 25 °C. For all proteins the absorbance recorded at the end of the reaction was 0.20. In the absence of protein (f) the decrease in absorbance reflects precipitation of the Fe(III) hydroxide micelles.

tion in accord with binding of 12 Fe(II) to these variants. Little H^+ production is observed for the double and triple mutants H31G-H43G and H31G-H43G-D58A (Table 4).

Fe(III) Binding. To determine the stoichiometry of Fe(III) binding to *Listeria* Dps, a careful fluorescence titration with Fe(II) was carried out anaerobically with additions of 4 Fe(II)/protein, followed by addition of 0.5 H_2O_2/Fe(II) each time. Fe(III) quenching of tryptophan fluorescence has both paramagnetic and resonance energy transfer components (*25*) owing to the overlap of the emission spectrum of tryptophan with the absorption spectrum of the hydrolyzed Fe(III). The quenching of the intrinsic fluorescence upon Fe(II) binding and oxidation shows a discontinuity at 22.7 Fe(III)/dodecamer (Figure 4), indicating ~24 Fe(III) binding sites on the protein shell, 2 sites per subunit.

Subsequently, the same experiments were performed for the ferroxidase center variants. The Fe(III)/protein stoichiometries obtained for H31G, H43G, the double and triple mutants were 21.3, 21.6, 22.1, and 24.2, respectively. As the number of mutated ferroxidase center residues increases, the extent of fluorescence quenching arising from Fe(III) binding decreases and the end point near 24 Fe(III)/dodecamer becomes less distinct (Figure 4), in accord with decreased occupation of the ferroxidase center with Fe(III).

Kinetics of Fe(II) Oxidation and Mineralization. In a first set of experiments molecular oxygen was used as oxidant. The rate of Fe(II) oxidation at the ferroxidase center was measured after addition of 12 or 24 Fe(II)/dodecamer to the wt and variant proteins (6.0 μM) in 50 mM Mops−NaOH, pH 7.0. The initial rates and the progress curves of iron oxidation monitored from the increase in absorbance at 310 nm show minimal differences (Figure 5). In particular, the initial rates do not differ significantly from Fe(II) autoxidation (Figure 5B). No significant differences are observed when the iron added amounts to 150 and 400 Fe(II)/dodecamer, and the kinetics of mineralization is followed at 310 nm or the distribution of the micellar iron core is assessed by sedimentation velocity. Thus, the sedimentation profile of all proteins under study loaded with 150 Fe(II)/dodecamer (about one-third of the maximum capacity) shows a slow-moving peak pertaining to the apoprotein ($s_{20,w} \sim 10.5$ S) and a faster moving peak pertaining to the iron-containing protein ($s_{20,w} \sim 17-20$ S). In the triple mutant an additional peak ($s_{20,w} \sim 30$ S) ascribable to iron aggregates is observed (data not shown).

A second set of kinetic experiments was performed in the presence of H_2O_2, which has been shown to carry out Fe(II) oxidation more efficiently than O_2 in *Listeria* Dps (*23*). Experiments of Fe(II) oxidation with the *Listeria* Dps variants were performed anaerobically by adding H_2O_2 immediately after 12 Fe(II)/dodecamer. The measured initial rates versus the amount of iron loaded are plotted in Figure 6. For the first two injections of 12 Fe(II)/dodecamer, compared to the wt protein (curve a, first two points), all of the variants display greatly attenuated initial rates (curves b−e, first two

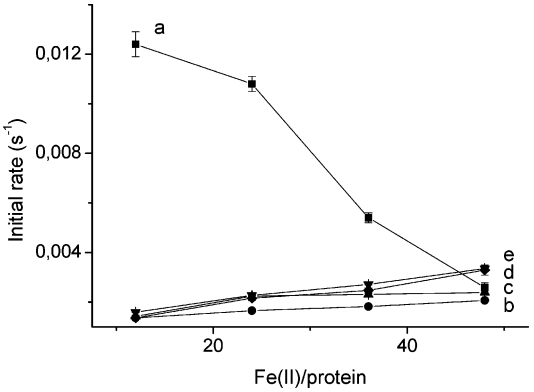

FIGURE 6: Initial rates of Fe(II) oxidation by H_2O_2 in *L. innocua* Dps and its ferroxidase center variants. Curves: (a, ■) wt Dps, 1.1 μM; (b, ●) H31G, 0.86 μM; (c, ▲) H43G, 1.1 μM; (d, ▼) H31G-H43G, 1.0 μM; (e, ◆) H31G-H43G-D58A, 1.1 μM. Each point corresponds to an addition of 12 Fe(II)/dodecamer followed by 0.5 H_2O_2/Fe(II). Conditions: anaerobic, 0.1 M Mops, 0.05 M NaCl, pH 7.0. The initial rates correspond to the linear a_1 term from a third-order polynomial fit to the absorbance at 304 nm vs time curves as detailed in ref *23*.

points), indicating decreased ferroxidase activity and the involvement of His31 and His43 (and probably Asp58) in catalysis. The initial rate for the wt protein falls off dramatically after addition of 24 Fe(II)/dodecamer, becoming comparable to the variants by addition of 48 Fe(II)/dodecamer, where mineralization is operative in all of the proteins (Figure 6).

DNA Protection Assays. To establish whether the site-specific mutations introduced at the ferroxidase center affect the DNA protection capacity of *L. innocua* Dps, an in vitro DNA damage assay was used (*23*). The combined effect of 10 mM H_2O_2 and Fe(II) at different concentrations on the integrity of plasmid pET-11a (5600 bp) was assessed in the presence and absence of protein (3 μM). At 24 Fe/dodecamer, there is no significant difference in the protection afforded by the wild-type protein and the variants (data not shown). However, at 96 Fe/dodecamer (Figure 7) the double (lane 4) and triple (lane 5) mutants protect DNA roughly one-third as efficiently as the wild-type protein (lane 3). The H31G and H43G mutants protect DNA about 10% less than the wild-type protein (data not shown). When the amount of iron is increased further to 192 Fe/dodecamer, the wt protein is still capable of protecting DNA, albeit to a lesser extent than at the lower Fe(II) concentration (lane 6 vs lane 3), whereas the double (lane 7) and triple (lane 8) mutants are unable to afford protection.

The capacity of wt *Listeria* Dps and its variants to quench the Fe(II)-mediated production of hydroxyl radicals with H_2O_2 as the oxidant was assessed also by means of a fluorometric assay that measures the degradation of deoxyribose to a fluorescent chromogen induced by such radicals (*4*, *24*). At 100 Fe(II)/dodecamer, about 41% degradation of deoxyribose is obtained in the presence of the wt protein. The extent of degradation is 47−45% for the H31G and H43G mutants and increases to 76−82% for the double and triple mutants. It follows that the mutants inhibit degradation 35−42% less efficiently than the wt protein, in accord with the data presented in Figure 7.

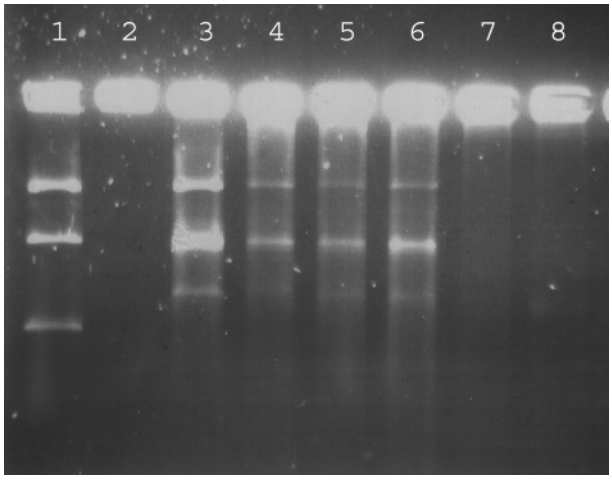

FIGURE 7: DNA protection by *L. innocua* Dps and the H31G-H43G and H31G-H43G-D58A variants. All reaction mixtures contained 20 nM pET-11a. Lanes: 1, plasmid DNA exposed to 10 mM H_2O_2; 2, plasmid DNA exposed first to 288 μM $FeSO_4$ and then to 10 mM H_2O_2; 3, plasmid DNA with 3 μM *Listeria* Dps exposed first to 288 μM $FeSO_4$ and then to 10 mM H_2O_2; 4, conditions as in lane 3 but with 3 μM H31G-H43G; 5, conditions as in lanes 3 and 4 but with 3 μM H31G-H43G-D58A; 6, plasmid DNA with 3 μM *Listeria* Dps exposed to 576 μM $FeSO_4$ and then to 10 mM H_2O_2; 7, conditions as in lane 6 but with 3 μM H31G-H43G; 8, conditions as in lanes 6 and 7 but with 3 μM H31G-H43G-D58A.

DISCUSSION

The ferroxidase centers in Dps proteins are unusual not only for the intersubunit location but also because the ferroxidation reaction has distinctive features compared to canonical ferritins. The present site-directed mutagenesis study on *L. innocua* Dps, where the ferroxidase center was first described and characterized (*10*, *12*), provides insight into the role played by specific iron ligands and by the ferroxidase center itself in the iron oxidation/uptake process and in hydrogen peroxide detoxification.

Ferroxidase activity requires binding of two Fe(II) to the A and B site of the catalytic center and depends on the multiplicity of iron−protein interactions thereby established. In canonical ferritins only the A site harbors a histidine residue, whereas in *Listeria* Dps this relatively strong iron ligand is present in both the A and B sites which host His31 and His43, respectively (*10*). The X-ray crystal structure of the native protein shows that these two histidine residues have a different affinity for iron in its oxidized state. Thus, His31 is ligated to iron at the A site, where metal coordination involves also Asp58, Glu62, and a water molecule (Wb), which in turn is hydrogen bonded to His43. In the modeled bimetallic center, the B site iron replaces this water molecule, and the iron coordination sphere comprises Glu62 that provides a bridging ligand to Wb. Interestingly, in most Dps structures where iron is present, Wb is conserved just as the interactions it establishes with the A site iron and His43, a conserved amino acid among the family members (*4*, *26*).

The X-ray crystal structures of the mutant proteins display small, yet significant changes in the ferroxidase center region with respect to native *Listeria* Dps (Figure 2) with no significant alterations in the conformation of the subunits or in their arrangement in the protein shell. Accordingly, the circular dichroic properties are essentially unaffected by the ferroxidase center mutations (Figure 1). In the H31G variant,

removal of His31 results in the loss of bound iron that is replaced by a water molecule (Wa) which occupies the ferroxidase center in addition to Wb. Consequently, an extended hydrogen bond network is formed comprising the two water molecules, the iron ligands, Asp58 (OD2), Glu62 (OE2), and His43, and in addition Asp47 (OD1), which is closer to Asp58 and Glu62 than in native Dps. A further hydrogen bond is established between Wb and His43 although these residues are further apart than in the native protein. The presence of His43 appears to be essential for the stabilization of this hydrogen bond network and for the binding of Wa and Wb. Thus, in H43G and in the double mutant H31G-H43G the ferroxidase center contains no iron or water molecules such that the iron ligands, being free from hydrogen-bonding interactions, undergo small movements or have different side chain arrangements relative to the native protein. In the H43G mutant, for example, Glu62 moves away from Lys141, and the Asp58 side chain can adopt two different conformations. One resembles that of the native protein, despite the absence of the metal ion, due to hydrogen bonding to Trp32 and Glu62. The other conformation, where Asp58 is hydrogen bonded to Gly54 and His28, resembles that of *E. coli* Dps where a lysine residue (Lys48) occupies the position of His28 (*4*). In the variants, therefore, the side chain movements are restricted to the carboxylate residues whereas the positioning of the His31 and His43 residues remains essentially unaltered. Previous work on *A. tumefaciens* and *Bacillus. brevis* Dps in their iron-free and iron-containing forms likewise evidenced the conformational flexibility of the Asp58 and Asp47 side chains (*4*, *27*). Taken together, these observations indicate that the A and B sites are essentially preformed and that metal binding does not require extensive ligand movement, just as in the ferroxidase centers of canonical ferritins (*13*, *14*). The mobility of the negatively charged side chains is likely to be used by *Listeria* Dps also to ensure movement of iron to and from the ferroxidase center. In particular, Asp47 and the nearby Glu44, which face the internal cavity of the protein shell, could play a role in nucleation of the iron micelle. In the H31G variant, however, Asp47 may substitute the mutated H31 residue in the ligation of iron since it is hydrogen bonded to both Wa and Wb, which occupy the position of the protein-bound iron in native *Listeria* Dps.

Intriguingly, the rather similar affinity ($\sim 10^5$ M^{-1}) of the H43G and H31G variants for Fe(II) is an indication that both His31 and His43 are capable of coordinating Fe(II) individually with modest affinity. The liberation of a single proton in the single mutants H31G and H43G suggests that the unaltered His residue where Fe(II) binds is the likely source of the proton in each case. The binding of 12 Fe(II)/dodecamer in the wt protein with the higher affinity ($\sim 10^7$ M^{-1}; see also ref *23*) probably occurs at His31, based on the fluorescence quenching data of Figure 3 (curve c) and on the X-ray structure showing occupancy of this site by iron (*10*). However, the possibility that binding occurs at either His31 or His43 to give one Fe(II) complexed per ferroxidase center or solely at His43 is not precluded by the data. The 100-fold reduction in binding affinity associated with either single mutation corresponds to a loss of ~3 kcal/mol in free energy of binding compared to the wt protein and indicates that the A and B sites of the ferroxidase center do not act in isolation but rather have some influence on one another.

In the double and triple mutants binding of Fe(II) to the ferroxidase center does not take place based on the titration experiments depicted in Figure 3. Thus, the small amount of protons released (Table 4) can be taken to result from nonspecific binding of Fe(II) that may proceed directly toward the carboxylate ligands involved in core nucleation due to the drastically decreased affinity of the ferroxidase center for the metal. In this connection it may be recalled that, in the native protein, Asp47 and Glu44, two carboxylates facing the internal protein surface, are located near His43.

The different extent of quenching of the protein fluorescence in the H31G and H43G variants attendant Fe(II) binding deserves comment. The significantly stronger quenching of the protein fluorescence observed in the H43G mutant relative to the H31G variant cannot be easily accounted for since the small alterations in the ferroxidase center do not alter the distances between either Trp32 or Trp144 and the protein-bound Fe in the variants compared to the native protein. Small conformational changes undetected by X-ray crystallography may be invoked. As expected from the involvement of carboxylate residues as iron ligands, when iron is oxidized immediately after binding, the apparent stoichiometry of the reaction corresponds to 24 ions/dodecamer both in the wt protein and in the H43G and H31G mutants (Figure 4). In the double and triple mutants the stoichiometry is less distinct, again in accord with nonspecific binding.

The functional ramifications of the ferroxidase center mutations differ dramatically depending on the nature of the oxidant. In the presence of dioxygen, in accord with the scarce efficacy of this oxidant (*12*), little or no effect of the mutations is apparent in the kinetics of the oxidation process (Figure 5) and in the size and distribution of the iron micelles formed inside the protein shell. In contrast, in the presence of hydrogen peroxide in the mutants the kinetics of iron oxidation decreases markedly (Figure 6), and the capacity to inhibit Fenton chemistry, and hence to protect DNA from oxidative damage, appears increasingly compromised with increase in iron concentration and in the number of mutated residues (Figure 7).

In conclusion, the behavior of the ferroxidase center variants of *Listeria* Dps shows that an intact ferroxidase center is not required when the bacterium is in an aerobic environment but is necessary to withstand the damaging effects of hydrogen peroxide and provides yet another proof that the biological role of ferroxidation in Dps proteins is related to peroxide tolerance.

REFERENCES

1. Bozzi, M., Mignogna, G., Stefanini, S., Barra, D., Longhi, C., Valenti, P., and Chiancone, E. (1997) A novel non-heme iron-binding ferritin related to the DNA-binding proteins of the Dps family in *Listeria innocua*, *J. Biol. Chem. 272*, 3259−3265.
2. Papinutto, E., Dundon, W. G., Pitulis, N., Battistutta, R., Montecucco, C., and Zanotti, G. (2002) Structure of two iron-binding proteins from *Bacillus anthracis*, *J. Biol. Chem. 277*, 15093−15098.
3. Zanotti, G., Papinutto, E., Dundon, W. G., Battistutta, R., Seveso, M., Del Giudice, G., Rappuoli, R., and Montecucco, C. (2002) Structure of the neutrophil-activating protein from *Helicobacter pylori*, *J. Mol. Biol. 323*, 125−130.

4. Ceci, P., Ilari, A., Falvo, E., and Chiancone, E. (2003) The Dps protein of *Agrobacterium tumefaciens* does not bind to DNA but protects it toward oxidative cleavage: x-ray crystal structure, iron binding, and hydroxyl-radical scavenging properties, *J. Biol. Chem. 278*, 20319−20326.
5. Halsey, T. A., Vazquez-Torres, A., Gravdahl, D. J., Fang, F. C., and Libby, S. J. (2004) The ferritin-like Dps protein is required for *Salmonella enterica* serovar *typhimurium* oxidative stress resistance and virulence, *Infect. Immun. 72*, 1155−1158.
6. Cooksley, C., Jenks, P. J., Green, A., Cockayne, A., Logan, R. P., and Hardie, K. R. (2003) NapA protects *Helicobacter pylori* from oxidative stress damage, and its production is influenced by the ferric uptake regulator, *J. Med. Microbiol. 6*, 461−469.
7. Ishikawa, T., Mizunoe, Y., Kawabata, S., Takade, A., Harada, M., Wai, S. N., and Yoshida, S. (2003) The iron-binding protein Dps confers hydrogen peroxide stress resistance to *Campylobacter jejuni*, *J. Bacteriol. 185*, 1010−1017.
8. Ueshima, J., Shoji, M., Ratnayake, D. B., Abe, K., Yoshida, S., Yamamoto, K., and Nakayama, K. (2003) Purification, gene cloning, gene expression, and mutants of Dps from the obligate anaerobe *Porphyromonas gingivalis*, *Infect. Immun. 71*, 1170−1178.
9. Pulliainen, A. T., Haataja, S., Kahkonen, S., and Finne, J. (2003) Molecular basis of H_2O_2 resistance mediated by streptococcal Dpr. Demonstration of the functional involvement of the putative ferroxidase center by site-directed mutagenesis in *Streptococcus suis*, *J. Biol. Chem. 278*, 7996−8005.
10. Ilari, A., Stefanini, S., Chiancone, E., and Tsernoglou, D. (2000) The dodecameric ferritin from *Listeria innocua* contains a novel intersubunit iron-binding site, *Nat. Struct. Biol. 7*, 38−43.
11. Ilari, A., Ceci, P., Ferrari, D., Rossi, G. L., and Chiancone, E. (2002) Iron incorporation into *Escherichia coli* Dps gives rise to a ferritin-like microcrystalline core, *J. Biol. Chem. 277*, 37619−37623.
12. Yang, X., Chiancone, E., Stefanini, S., Ilari, A., and Chasteen, N. D. (2000) Iron oxidation and hydrolysis reactions of a novel ferritin from *Listeria innocua*, *Biochem. J. 349*, 783−786.
13. Treffry, A., Zhao, Z., Quail, M.A., Guest, J. R., and Harrison, P. M. (1997) Dinuclear center of ferritin: studies of iron binding and oxidation show differences in the two iron sites, *Biochemistry 36*, 432−441.
14. Bou-Abdallah, F., Arosio, P., Santambrogio, P., Yang, X., Janus-Chandler C., and Chasteen, N. D. (2002) Ferrous ion binding to recombinant human H-chain ferritin. An isothermal titration calorimetry study, *Biochemistry 41*, 11184−11191.
15. Polidoro, M., De Biase, D., Montagnini, B., Guarrera, L., Cavallo, S., Valenti, P., Stefanini, S., and Chiancone, E. (2002) The expression of the dodecameric ferritin in *Listeria* spp. is induced by iron limitation and stationary growth phase, *Gene 296*, 121−128.
16. Otwinowski, Z., and Minor, W. (1997) Processing of X-ray diffraction data collected in oscillation mode, *Methods Enzymol. 276*, 307−326.
17. Navaza, J. (1994) AmoRe: an automated package for molecular replacement, *Acta Crystallogr. A50*, 157−163.
18. Murshudov, G. N., Vagin, A., Lebedev, A., Wilson, K. S., and Dodson, E. J. (1999) Efficient anisotropic refinement of macromolecular structures using FFT, *Acta Crystallogr. D55*, 247−255.
19. McRee, D. E. (1993) in *Practical Protein Crystallography*, pp 365−374, Academic Press, Orlando, FL.
20. Laskowski, R. A., McArthur, M. W., Moss, D. S., and Thornton (1993) Procheck: a program to check the stereochemical quality of protein structures, *J. Appl. Crystallogr. 26*, 283−291.
21. Yang, X., Chen-Barret, Y., Arosio, P., and Chasteen N. D. (1998) Reaction paths of iron oxidation and hydrolysis in horse spleen and recombinant human ferritins, *Biochemistry 37*, 9743−9750.
22. Macara, I. G., Hoy, T. G., and Harrison, P. M. (1972) The formation of ferritin from apoferritin. Kinetics and mechanism of iron uptake, *Biochem. J. 126*, 151−162.
23. Su, M., Cavallo, S., Stefanini, S., Chiancone, E., and Chasteen, N. D. (2005) The so-called *Listeria innocua* ferritin is a Dps protein. Iron incorporation-detoxification and DNA protection properties, *Biochemistry 44*, 5572−5578.
24. Yamamoto, Y., Poole, L. B., Hantgan, R. R., and Kamio, Y. (2002) An iron-binding protein, Dpr, from *Streptococcus mutans* prevents iron-dependent hydroxyl radical formation in vitro, *J. Bacteriol. 184*, 2931−2939.
25. Förster, T. H. (1948) Zwischenmolekulare Energiewanderung und Fluoreszenz, *Ann. Phys. 2*, 55−77.
26. Zeth, K., Offermann, S., Essen, L. O., and Oesterhelt, D. **(**2004) Iron-oxo clusters biomineralizing on protein surfaces: structural analysis of *Halobacterium salinarum* DpsA in its low- and high-iron states, *Proc. Natl. Acad. Sci. U.S.A. 101*, 13780−13785.
27. Ren, B., Tibbelin, G., Kajino, T., Asami, O., and Ladenstein, R. (2003) The multi-layered structure of Dps with a novel di-nuclear ferroxidase center, *J. Mol. Biol. 329*, 467−477.
28. Delano, W. L. (1998−2003) *The PyMOL Molecular Graphics System*, Delano Scientific LLC, San Carlos, LA (http://www.pymol.org).

BI050005E